ONLINE FIRST

This is a provisional PDF only. Copyedited and fully formatted versión will be made available at final publication

HISTOLOGY AND HISTOPATHOLOGY

ISSN: 0213-3911
e-ISSN: 1699-5848

Submit your article to this Journal (http://www.hh.um.es/Instructions.htm)

Cold-shock proteins accumulate in centrosomes and their expression and primary cilium morphology are regulated by hypothermia and shear stress

Authors: María Díaz de Cerio, Sara Oliván, Ignacio Ochoa, Josune García-Sanmartín and Alfredo Martínez

DOI: 10.14670/HH-18-656
Article type: ORIGINAL ARTICLE
Accepted: 2023-08-03
Epub ahead of print: 2023-08-03

Cold-shock proteins accumulate in centrosomes and their expression and primary cilium morphology are regulated by hypothermia and shear stress

María Díaz de Cerio[1], Sara Oliván[2], Ignacio Ochoa[2,3], Josune García-Sanmartín[1], Alfredo Martínez[1,*]

[1]Angiogenesis Unit, Oncology Area, Center for Biomedical Research of La Rioja (CIBIR), 26006 Logroño, Spain.

[2] Tissue Microenvironment Lab (TMELab), University of Zaragoza, Aragón Institute of Engineering Research (I3A), 50018 Zaragoza, Spain.

[3] Centro de Investigación Biomédica en Red. Bioingeniería, Biomateriales y Nanomedicina (CIBER-BBN), Institute for Health Research Aragon (IIS Aragón), 50018 Zaragoza, Spain.

[*]Correspondence: amartinezr@riojasalud.es

Keywords: Primary cilium; centrosome; cold-shock proteins; CIRP; RBM3; hypothermia; shear stress.

Short title: The primary cilium as a sensor for cold.

Abstract

Primary cilia act as cellular sensors for multiple extracellular stimuli and regulate many intracellular signaling pathways in response. Here we investigate whether the cold-shock proteins (CSPs), CIRP and RBM3, are present in the primary cilia and the physiological consequences of such a relationship. R28, an immortalized retinal precursor cell line, was stained with antibodies against CIRP, RBM3, and ciliary markers. Both CSPs were found in intimate contact with the basal body of the cilium during all stages of the cell cycle, including migrating with the centrosome during mitosis. In addition, the morphological and physiological manifestations of exposing the cells to hypothermia and shear stress were investigated. Exposure to moderately cold (32°C) temperatures, the hypothermia mimetic small molecule zr17-2, or to shear stress resulted in a significant reduction in the number and length of primary cilia. In addition, shear stress induced expression of CIRP and RBM3 in a complex pattern depending on the specific protein, flow intensity, and type of flow (laminar versus oscillatory). Flow-mediated CSP overexpression was detected by qRT-PCR and confirmed by Western blot, at least for CIRP. Furthermore, analysis of public RNA Seq databases on flow experiments confirmed an increase of CIRP and RBM3 expression following exposure to shear stress in renal cell lines. In conclusion, we found that CSPs are integral components of the centrosome and that they participate in cold and shear stress sensing.

a. List of abbreviations

ANOVA: Analysis of variance

CIRP: Cold inducible RNA-binding protein

CPM: Counts per million.

CSP: Cold shock proteins

GPCR: G protein coupled receptors

hnRNP: Heterogeneous nuclear ribonucleoprotein

qRT-PCR: Quantitative real time polymerase chain reaction

RBM3: RNA-binding protein 3

TGF: Transforming growth factor

Introduction

Primary cilia are non-motile antenna-like structures that are present in most mammalian cells. This structure acts as a sensor for multiple extracellular stimuli due to a unique membrane combination of lipids and receptors (Anvarian et al., 2019). When initially discovered, 60 years ago, the primary cilium was considered a vestigial structure (Sorokin, 1962) but today we know that it plays a major role in regulating multiple signal pathways, including Hedgehog, Wingless, G protein coupled receptors (GPCR), and many others (Wheway et al., 2018). In fact, defects in primary cilium development are responsible for a number of conditions known as ciliopathies, which may affect many organs (Hildebrandt et al., 2011).

Morphologically, the primary cilium is between 250-300 nm in diameter, and 1-10 µm in length (Wang et al., 2021a) The primary cilium is composed of the basal body, from which a membrane-covered axoneme of nine microtubule duplets (9 + 0) extends outward from the cell (Chen et al., 2021). The ciliary membrane is continuous with the cellular membrane although the composition regarding lipids and proteins is quite different (Garcia et al., 2018). At the base of the primary cilium is the basal body, which originates from the mother centriole and, together with the daughter centriole and the pericentriolar matrix, forms the centrosome, the microtubule organizing center of the cell (Wilsch-Brauninger and Huttner, 2021). In contrast with motile cilia, which have a very conserved structure, primary cilia present a more diverse architecture and protein composition, which may be adaptations for specific functions (Pigino, 2021). As many signaling systems have been located in primary cilia and an increasing number of proteins have been identified that localize to the different substructures of the cilium and basal body (Wilsch-Brauninger and Huttner, 2021), we should expect new examples to be discovered in the near future. Between the basal body and the axoneme, we find the transition zone. This is an important area since it controls the entry and exit of ciliary proteins, thus contributing to ciliary compartmentalization (Anvarian et al., 2019). All ciliary proteins are synthesized in the cell´s cytoplasm and need to be transported into the cilium. Once inside, they reach their final destination by means of the intraflagellar transport, which may be anterograde (driven by kinesin-2) or retrograde (driven by dynein-2) (Pigino, 2021).

These characteristics make the primary cilium a main sensing and signaling organelle in the cell. The contents of signaling elements inside the cilium are very dynamic and are closely related with the stages of cell differentiation and the microenvironment (Heydeck et al., 2018). Primary cilia signaling is paramount during development and in stem cell maintenance, as demonstrated by the deleterious results of ciliopathies (Andreu-Cervera et al., 2021), but they are also relevant in the adult organism. For instance, primary cilia in the tubular system of nephrons are able to sense modifications in urine composition and osmolality, modulating important intracellular signaling pathways such as Wnt (Goggolidou, 2014) or Hippo (Habbig et al., 2011). Another function of primary cilia in adult individuals is their role as molecular mechanosensors able to sense differences in fluid (blood, urine, bile, cerebrospinal fluid, etc) flow (Spasic and Jacobs, 2017). The primary cilia are not just passive mechanosensors, but they can modulate themselves depending on the surrounding stimuli. For instance, they can modify their cytoskeleton to better support shear stress (Spasic and Jacobs, 2017). They can also modify their rigidity, rotation, and length to adapt to their environment (Espinha et al., 2014). In addition, their size and number are related to the intensity of blood flow in endothelial cells and are characteristic of each region of the arterial tree (Wang et al., 2021b).

The primary cilium disassembles when the cell enters mitosis, releasing the basal body into the cytoplasm. During the G1/S phase of the cell cycle the centrioles separate and duplicate to form a new pair of centrioles, which generate one centrosome each. These centrosomes separate during mitosis and migrate apart to form the spindle poles (Wilsch-Brauninger and Huttner, 2021). As cells enter mitosis, centrosomes dramatically increase in size and ability to nucleate microtubules. This process, termed centrosome maturation, is driven by the accumulation and activation of γ-tubulin and other proteins that form the pericentriolar material on centrosomes during G2/prophase (Gomez-Ferreria et al., 2007). After mitosis, the mother centriole of each daughter cell anchors to the membrane and regrows a primary cilium by extending the axonemal microtubules, formation of the transition zone, and establishment of the intraflagellar transport (Liu et al., 2018).

More centrosomal proteins involved in different aspects of centrosome function are being characterized every day. Many of them have multiple properties for different parameters such as localization, timing, and activity. For example, proteins, such as tubulin, can be found localized in both centrioles as well as in pericentriolar material or in the axoneme of the cilia. In terms of timing, while some proteins are always present in the centrosome, other proteins only appear in the centrosome at a particular stage of cell differentiation or at certain times in the cell cycle, such as Cep192 (Gomez-Ferreria et al., 2007). In any case, centrosomal proteins do not normally exist on their own, but rather as complexes that are often interconnected as functional complexes, as recently reviewed in more detail elsewhere (Uzbekov and Avidor-Reiss, 2020).

Cold-shock proteins (CSP) are a small group of proteins whose expression increases under exposure to moderately cold temperatures (hypothermia). In mammals, there are two main CSPs, cold inducible RNA-binding protein (CIRP) and RNA-binding protein 3 (RBM3). These proteins belong to the heterogeneous nuclear ribonucleoprotein family, bind to cellular RNAs and regulate their half-life and thus their expression and final function (Wellmann et al., 2004; Lleonart 2010; Wellmann et al., 2010; Liu et al., 2013). The mRNAs that bind to these proteins are usually related to cell survival (Zhang et al., 2015; Wu et al., 2017), thus implying this system in the benefits provided by therapeutic hypothermia (Rey-Funes et al., 2017). Recently, we have developed a group of small molecules that bind to CIRP and increase its protein expression (Coderch et al., 2017), and therefore can be considered hypothermia mimetics. In fact, they have been applied *in vivo* and induce organ protection similar to hypothermia (Contartese et al., 2023).

Interestingly, in a recent report, the presence of RNA-binding proteins has been localized in centrosomes, identifying these structures as active sites of protein synthesis (Zein-Sabatto and Lerit, 2021). Based on these observations, we hypothesized that CSPs may be located in primary cilia where they may play important roles in sensing temperature changes and other chemical or mechanic stimuli.

Materials and methods

Cell line and culture conditions

Immortalized rat retinal precursor cell line R28 (RRID:CVCL_5135) was a gift from Dr. Patricia Becerra (National Eye Institute, NIH, Bethesda, MD, USA and was established from a 6-day-old rat retinal culture (Seigel, 2014). From these precursors, most of the retinal neurons originate, including the photoreceptors, whose apical segments are modified primary cilia (Wheway et al., 2019). Furthermore, it was previously shown that R28 cells express CSPs and respond to hypothermia (Larrayoz et al., 2016; Coderch et al., 2017). R28 cells were cultured in DMEM medium supplemented with 10% fetal bovine serum (Invitrogen, Alcobendas, Spain) at 37°C in an atmosphere containing 5% CO_2. For hypothermia experiments, cells were maintained in the same conditions but at 32°C. This temperature was chosen since it is used routinely as a moderate hypothermic treatment in the clinic (Shah et al., 2007) and it has been shown to induce CIRP expression in cell line R28 (Larrayoz et al., 2016; Coderch et al., 2017). The hypothermia mimetic small molecule zr17-2 was synthesized in house, as described (Maslyk et al., 2010) and was applied to the cell cultures at a concentration of 10 µM, as described (Coderch et al., 2017).

Laminar flow

Experiments under flow to induce mechanical shear stress on cells were performed using microfluidic devices from BEOnChip (BE-Flow, Zaragoza, Spain). R28 cells were trypsinized and resuspended at the desired density ($2.5x10^6$ cells/ml) prior to injection into the different channels of the chips. Once seeded, they were incubated at 37°C and 5% CO_2 for 24 h to induce cell attachment to the chip surface. Once the cells formed a confluent monolayer, the microdevices were connected to a syringe pump (NE-1600, New Era, Farmingdale, NY, USA) to carry out the experiments under flow conditions. Different continuous flow pressures of culture medium (0, 15.5, 31, 62, and 124 µl/min, corresponding to 0, 0.2, 0.5, 1.0, and 2.0 dynes/cm^2, respectively) were applied for the indicated times. Cells destined for immunofluorescence were fixed in 10% buffered formalin, whereas those destined for qRT-PCR were dispersed in TRIzol and kept frozen at -80°C until further analysis (see below). All experiments were replicated three times, at least.

Oscillatory flow

To generate oscillatory flow conditions, R28 cells were seeded onto glass slides (SuperFrost Plus, Thermo Fisher Scientific, Waltham, MA, USA) until they reached full confluence. The slides were placed in plastic dishes (100 mm in diameter), containing 10 ml of culture medium, that were deposited on a rocking platform (Rocking Shaker, Ohaus, Nänikon, Switzerland), configured with a maximum inclination of 5 degrees and a frequency of 10 rpm, inside a cell culture incubator. These conditions produce a maximum turbulent flow of approximately 0.81 dynes/cm^2. Control plates were placed in the same incubator with no movement. Cells were exposed to shear stress for different time periods and they were collected for either qRT-PCR or Western blotting by scraping the cells in the proper lysis buffer (see below). All experiments were replicated three times, at least.

Confocal microscopy and quantification of morphological characteristics

Cells were cultured in glass slides or coverslips overnight, exposed to cold or flow conditions for the indicated times, fixed with 10% buffered formalin for 10 min, permeabilized with 0.1% triton X-100 in PBS for 10 min, and exposed to a mix of primary antibodies (Table 1) overnight at 4°C. These primary antibodies included rabbit immunoglobulins against CIRP or RBM3, and mouse anti-acetylated tubulin, as a marker of the ciliary axoneme (Shida et al., 2010). Following vigorous washes, a mix of fluorescently labeled secondary antibodies (Alexa 647 anti-rabbit and CF543 anti-mouse, Table 1) were added for 1 h at room temperature. Then, potential mouse IgG binding sites were blocked by incubation with Fab fragment donkey anti-mouse IgG for 1 h, followed by fluorescently (Alexa 488) labeled γ-tubulin as a centrosome marker (Hagiwara et al., 2000) for another hour. After another series of washes and an incubation with Hoechst (1:2,000) as a nuclear counterstain, the coverslips were mounted on glass slides (or vice versa). Controls included omission of a primary antibody at a time. A confocal microscope (Leica TCS SP5, Leica, Badalona, Spain) was used to visualize the slides. The Leica software package was used to quantify the number, length, and staining intensity of the primary cilia. Specifically, the length of the acetylated-tubulin-positive axonemes was

measured with the proper tools in the LAS X software suite (Leica) in cilia with an orientation parallel to the slide.

All used antibodies have been previously used and characterized: CIRP (Coderch et al., 2017), RBM3 (Larrayoz et al., 2016), γ-tubulin (Roberts et al., 2020), and acetylated tubulin (Smith et al., 2018).

All experiments were performed at least in triplicate, and a minimum of six fields per slide were analyzed. This represents a number of individual cells ranging from 3,761 to 7,083 per experimental condition. In terms of image manipulation, we have performed adjustments of brightness and contrast of the whole images to improve the visibility of the different fluorophores without obscuring, eliminating, or misrepresenting any information present in the original. The same adjustments were performed for the control samples. Both image processing and image adjustment were performed using LAS AF software (Leica). No specific feature within an image was enhanced, obscured, moved, removed or introduced.

mRNA extraction and gene expression quantification

Total RNA was isolated from cell cultures using TRIzol (Invitrogen, Waltham, MA, USA), purified using an RNeasy Micro kit (Qiagen, Valencia, CA, USA), and treated with DNase I (Qiagen) following the manufacturer's instructions. cDNA was synthesized by reverse transcription of 1 µg of total RNA using the SuperScript VILO Master Mix (Invitrogen) in a total volume of 20 µl according to the manufacturer's instructions. cDNA was amplified by qRT-PCR using Power SYBR Green PCR Master Mix (Applied Biosystems, Bedford, MA, USA) and specific primers (Table 2) in a QuantStudio 5 real time PCR system (Applied Biosystems). Gene expression was calculated by interpolation into a standard curve. All values were divided by the expression of the house keeping gene, GAPDH.

Protein extraction and Western blotting

Treated cells were lysed in M-PER buffer (Thermo Fisher Scientific) supplemented with cOmplete ULTRA protease inhibitor cocktail (Roche Diagnostics, Basel, Switzerland). The protein content of the lysates was quantified using the Bradford Protein Assay (BioRad, Hercules, CA, USA). Nupage sample reducing buffer (Invitrogen) was added to the lysates (30 µg), heated at 70 °C for 10 min, and separated by SDS polyacrylamide gel electrophoresis in 4–12% Bis-Tris gels (Invitrogen). Electrophoresed proteins were transferred to PVDF membranes using the iBlot 2 Transfer Device (Invitrogen). Once transferred, the membranes were blocked using 1% powder skim milk in Tris-buffered saline–Tween-20 (TBST; 25 mM Tris, pH 7.5, 150 mM NaCl, 0.1% (v/v) Tween-20). Membranes were exposed overnight to the primary antibodies (Table 1). On the next day, horseradish peroxidase (HRP)-linked secondary antibodies (Table 1) were applied for 1 h at room temperature. Peroxidase activity was detected with ECL Prime Western Blotting Detection Reagent (Cytiva, Marlborough, MA, USA) and captured in a ChemiDoc MP Imaging System (BioRad). The quantification of the immunoreactive bands was accomplished with the ImageLab software (BioRad). Tubulin was used as a loading control.

Data mining

Public repositories of RNASeq databases were searched for studies performed on cells subjected to different flow conditions. Only three such studies were found (Qiao et al., 2016; Mohammed et al., 2018; Kunnen et al., 2018). All sequences in fastq format were reanalyzed following standard biostatistics protocols under an R environment (Larrayoz et al., 2012) to determine the relative expression of CIRP and RBM3 in each sample. After data normalization, results are expressed as counts per million (CPM).

Statistical analysis

All data sets were analyzed for normalcy and homoscedasticity. Normal data were analyzed by Student´s *t* test or ANOVA, followed by Tukey´s Multiple Comparison test. Non parametric data were analyzed with Kruskal-Wallis and Mann-Whitney´s *U* test. A p value < 0.05 was considered statistically significant. All tests were performed with GraphPad Prism version 5.02 (GraphPad Software, Inc. La Jolla, CA, USA).

Results

CIRP and RBM3 are located in the basal body of primary cilia. Confocal microscopy analysis of R28 cells shows that immunofluorescence for CIRP and RBM3 are found in the cell nucleus but also in the basal body of primary cilia (Fig. 1). Multiple immunofluorescence shows a complete colocalization of γ-tubulin, a marker of the basal body, and both CSPs. In addition, the fluorescence for acetylated tubulin, which labels the axoneme, clearly identifies these structures as primary cilia. Furthermore, when cells in different stages of the cell cycle are analyzed, a continuous colocalization of the CSPs with the basal body/centrosome is confirmed, independently of the cell cycle phase (Fig. 2). During mitosis, CSP nuclear staining diminishes and gets distributed through the cytoplasm but the centrosome remains positive (Fig. 2).

Hypothermia reduces the number of primary cilia and their length. Since CSPs mediate the response to cold temperatures, we sought to analyze the impact of hypothermia on primary cilia by exposing R28 cells to 32°C (a 5°C drop from normal body temperature) for 96 h. In normal conditions (37°C), 39.3 ± 2.1 % of all cells possess a primary cilium but, after exposure to hypothermia, only 31.6 ± 8.0 % retained this structure (p=0.047) (Fig. 3). On the other hand, the length of the primary cilia decreased from 4.21 ± 1.11 µm in normothermia to 2.73 ± 0.74 µm in hypothermia (p=<0.0001) (Fig. 3). To demonstrate that therapeutic hypothermia increases CIRP expression, we performed a Western blot experiment and found a statistically significant increase when cells were cultivated at 32ºC (p=0.022) (Fig. 4a). In addition, to provide further support to the hypothesis that CIRP is the mediator between hypothermia and modifications of primary cilia morphology, we used the hypothermia mimetic zr17-2. This molecule has been shown to induce CIRP overexpression (Coderch et al. 2017). So, R28 cells were exposed to zr17-2 for 24 h and this treatment resulted in significant reductions in primary cilia number (Fig. 4b) and length (Fig. 4c), in a similar behavior to the one induced by hypothermia.

Laminar flow enhances CSP expression in primary cilia. Sensing and responding to shear stress is one of the main functions of primary cilia, so we investigated the influence of this mechanical stimulus on the localization and expression of CSPs in R28 cells. Figure 5 shows the impact of subjecting cells to a continuous flow of 124 µl/min (2.0 dynes/cm^2) for 8 h. Both CIRP (Fig. 5a) and RBM3 (Fig. 5b) remained associated to the basal bodies. When different flow intensities were tested, there was a reduction in the number of primary cilia for the slower flows (15 - 62 µL/min, $p<0.001$; $p=0.011$; $p=0.003$, respectively) but no significant change was found at the higher flow (124 µl/min) (Fig. 5c).

A gene expression analysis was performed by qRT-PCR using different flow intensities and times of exposure (Fig. 6). CIRP expression significantly rose after 1 and 2 h of exposure to a 31 µl/min (0.5 dynes/cm^2) flow and significantly decreased below control (static) values at 4 and 8 h. Expression levels returned to normal at 12 h (Fig. 6a). Surprisingly, no CIRP expression differences were found when cells were subjected to a 62 µl/min (1.0 dynes/cm^2) flow (Fig. 6a). On the other hand, RBM3 expression followed a different pattern, reaching a significant increase at 8 and 12 h with both flow intensities, returning to basal levels at 24h (Fig. 6b).

Oscillating flow enhances CSP expression in primary cilia. Primary cilia respond differently to laminar and to turbulent flow (Wang et al. 2021b). Therefore, we also investigated a model of turbulent flow by using an oscillating platform. Similarly to the results with laminar flow, both CIRP (Fig. 7a) and RBM3 (Fig. 7b) remained associated to the basal bodies of the primary cilia. In addition, after 2 h of rocking, there was a significant reduction in the number ($p=0.014$) and length ($p<0.0001$) of the primary cilia (Fig. 7c).

Quantification of CSP expression under these conditions was accomplished by qRT-PCR (Fig. 8a,b) and Western blotting (Fig. 8c,d). At the mRNA level, CIRP expression significantly increased at 1h ($p<0.0001$) and progressively decreased from there to normal levels (Fig. 8a). In this case, RBM3 expression changes were very similar to those of RBM3, reaching the zenith at 1 h ($p=0.001$), remaining significantly higher than the static control at 2 h ($p=0.017$) and coming back to normal at 6h (Fig. 8b). At the protein level, there was a significant increase in CIRP after 2 h of shear stress ($p=0.032$) but no significant differences were found at other times (Fig 8c). No changes were found for RBM3 protein at the conditions tested (Fig. 8d).

Data mining. In order to take advantage of previous RNA transcriptomic studies, we looked for datasets of shear stress experiments in public repositories to reveal unpublished changes in the expression of CIRP and RBM3. Only three studies fulfilled our search inclusion criteria and they were highly heterogeneous. Two of the studies were performed with laminar flow (Mohammed et al., 2018; Kunnen et al., 2018), whereas the other used oscillatory flow conditions (Qiao et al., 2016). There were also differences in the applied flow pressure: 0.6 dynes/cm^2 (Mohammed et al., 2018), 1.9 dynes/cm^2 (Kunnen et al., 2018), or 5.0 dynes/cm^2 (Qiao et al., 2016); and in the times of exposure: 3h, 6h, and 24h, respectively. At least, all cell lines were from the kidney (Fig. 9). In the 3h study, there was a significant increase for both CIRP ($p=0.015$) and RBM3 ($p=0.016$) in the cells exposed to shear stress. In the 6h manuscript, no differences in CIRP were appreciated whereas there was a significant increase in RBM3 ($p=0.031$). Finally, in the 24 h report, no changes were found in CIRP expression but there was a significant reduction in RBM3 ($p=0.022$) (Fig. 9).

Discussion

We have shown that the CSP proteins, CIRP and RBM3, colocalize with the basal body of the primary cilia in R28 cells, even during the M phase of the cell cycle. In addition, hypothermia and shear stress modulate the number and size of these organelles. Furthermore, application of shear stress (either laminar or turbulent flow) increases CSP expression in a time- and flow intensity-dependent manner.

R28 cells are undifferentiated retinal neuroblasts (Seigel, 2014). This is probably the first report of primary cilia in R28 cells, but the importance of this organelle in the retina is paramount since the outer segments of photoreceptors are basically modified primary cilia (Wheway et al., 2019). In addition, the eye responds very well to therapeutic hypothermia (Rey-Funes et al., 2017) and CSPs have been located in the retina (Larrayoz et al., 2016). According to our current results, more attention must be paid to the role of primary cilia in the ample applications of therapeutic hypothermia, especially in the field of vision-challenging conditions (Rey-Funes et al., 2021; Contartese et al., 2023).

An interesting observation is that CSPs are always associated to the centrosome in R28 cells, despite the severe changes caused by the cell cycle. The centrosome is a membraneless organelle that forms highly structured and stable macromolecular complexes, making it largely insoluble. This, together with the fact that most cells have only a single centrosome and a single cilium, is an inherent limitation in the study of these structures at the biochemical level (Arslanhan et al., 2020). Nevertheless, a recent study has been able to fully characterize the protein composition of the centrosome (O'Neill et al., 2022). Among the proteins found in the centrosomes of neural stem cells and of mature neurons, a large number of RNA binding proteins, including the heterogeneous nuclear ribonucleoprotein (hnRNP) family, were found.

CIRP and RBM3 belong to the hnRNP family, recognize specific RNA sequences, and are regulators of translation (Zhu et al., 2016). The centrosome is now considered a very active translation site (Lerit, 2022) and, therefore, the presence of CSPs in this cellular region is not unexpected. In fact, other RNA-binding proteins, such as Gle1 or CPEB, have also been described in centrosomes. Gle1 is a multifunctional regulator of RNA metabolism, best described for its role in mRNA transport, but also implicated in translation initiation and termination through DEAD-box proteins. Gle1 localizes to the centrosome and the basal body of cilia, colocalizes with pericentrin, and is required for the recruitment of pericentrin to the centrosome (Zein-Sabatto and Lerit, 2021). Furthermore, CSPs associate with the spliceosome (Barbosa-Morais et al., 2006) and some of the components of the spliceosome, including pre-RNA processing factors (PRPFs), have been found in the ciliary basal body or the centrosome, where they promote ciliogenesis (Wheway et al., 2015).

The behavior of centrosomal proteins during the cell cycle is variable and some of them may abandon the centrosome during mitosis whereas others remain within its limits. For instance, Cep192 is found attached to the centrosome during all phases of mitosis where it is an essential component of the centrosome maturation machinery (Gomez-Ferreria et al., 2007). In addition, Cep215 is always in association with the centrosome, both during interphase and mitosis (Graser et al., 2007). Obviously, CSPs have the same behavior as Cep215.

CSPs are also found in the cell nucleus during interphase, as all hnRNPs should be by definition. Depending on the environmental conditions, CSPs may migrate into the cytoplasm when exposed to hypothermia (Larrayoz et al., 2016) or to the stress granules following oxidative stress (De et al., 2007). During mitosis, and following nuclear membrane dissolution, we have

observed a dispersion of the nuclear CSP proteins into the cytoplasm, which would be incorporated back into the nuclei once the daughter cells develop their nuclear membranes. In clear contrast, the CSPs located in the centrosome remain associated to this structure throughout the whole cell cycle.

We have shown that hypothermia, hypothermia mimetics, or shear stress exposure results in a reduction in the number of primary cilia and a diminution of their length. Variations in the number of primary cilia are well known in the cardiovascular system, where there is a clear correlation with flow conditions; the number is lower in areas exposed to laminar flow whereas endothelial cells located in regions with more turbulent and oscillatory blood flow present more primary cilia (Dinsmore and Reiter, 2016). This is relevant since endothelial cells in disturbed flow areas are more exposed to inflammation and atherogenesis, and primary cilia protect them by blocking transforming growth factor (TGF) signaling and by secreting nitric oxide (Wang et al., 2021b). Furthermore, non-ciliated endothelial cells are more prone to endothelial-to-mesenchymal transition through activation of the SLUG pathway, thus increasing calcification and atherosclerosis risk (Sanchez-Duffhues et al., 2015). Therefore, it seems that lowering temperature has a similar effect to exposing the primary cilia to a less turbulent flow. In our data with laminar flow, there was a reduction in the number of primary cilia compared to the static cells, but the highest flow conditions (124 µl/min) had a number undistinguishable from the static cells, perhaps because this strong current induced some disturbances in the general flow conditions.

This is also consistent with the observation of a cold-induced size reduction of the primary cilium. In renal tubular epithelial cells, TGF-β signaling induces the shortening of primary cilia (Han et al., 2018). Thus, conditions leading to a reduction in the number of cilia, such as hypothermia, may also increase TGF signaling and decrease cilia length. The length of the primary cilium seems to be regulated by the activity of GPCRs, calcium levels, and actin depolymerization (Anvarian et al., 2019). Apparently, hypothermia blocks this mechanism, leading to cilia length reduction. A recent report has connected primary cilium shortening with a fragmentation mechanism (Park, 2018). Future studies will clarify which specific mechanism is triggered by hypothermia in the primary cilium.

It is well accepted that CIRP and RBM3 increase their expression in response to cold stimuli but they (and specially CIRP) also respond to other stresses, such as hypoxia (Lleonart, 2010; Zhu et al., 2016), UV light exposure (Baba et al., 2008), or cell damage (Rey-Funes et al., 2017). Therefore, it is not surprising to find CSPs in primary cilia where they may serve as chemical sensors for all those stimuli. In addition, the overexpression of CSPs has been related with the upregulation of antiapoptotic proteins such as BCL2 and/or a downregulation of proapoptotic proteins such as BAX, BAD, BAK, and others, protecting cells from programmed cell death (Zhang et al., 2015; Wu et al., 2017). It will be interesting to study the actual relationship between primary cilium-located CSPs and regulation of cell apoptosis.

Shear stress sensing is a critical mechanism to ensure proper circulation of fluids in the organism. For instance, endothelial cells are able to sense spatiotemporal characteristics of blood flow and therefore contribute to determine the morphofunctional properties of the vascular network by at least three kinds of mechanism, namely vessel regression and stabilization, long-term modulation of vessel diameter by inward and outward remodeling, and short-term vasoreactivity (Roux et al., 2020). This sensing function is carried out by the primary cilia (Luu et al., 2018), in combination with mechanotransductor molecules such as PIEZO1 and its downstream signaling cascade, which results in vasorelaxation (Iring et al., 2019). The

activation of CSP expression by shear stress is a new consequence of this mechanism whose physiological implications warrant further research.

We have shown that CSP expression is activated by shear stress, but the specific expression pattern depends on the protein under study and the kind of flow. For instance, with a laminar flow of 0.5 dynes/cm^2, we observed a fast upregulation of CIRP (at 1-2 h) whereas RBM3 expression increased only after 8-12 h of exposure. On the other hand, when oscillatory flow was applied, the expression of both CSPs reached a maximum at 1 h. Surprisingly, a higher flow (1.0 dynes/cm^2) did not induce CIRP expression but was able to upregulate RBM3. These observations suggest that the intimate interrelationship between shear stress and CSP expression regulation is very dependent on small details and that more in-depth studies are needed to better understand this interesting field. The RNA results were partially corroborated by Western blotting, at least for CIRP, whose protein expression was significantly elevated after 2 h of oscillatory flow. In the case of RBM3 we found no significant changes. We need to understand that the primary cilia represent a very small percentage of the cell´s total volume, so it is easy to miss protein changes that may be very relevant at the local level (primary cilia) but could be diluted with the rest of the cell´s contents. The data mining results, although collected from different cell systems, were also supportive of our experimental data. There was a significant shear stress-induced upregulation of both CIRP and RBM3 in the short term (3h), an overexpression of RBM3 in the midterm (6h), and even a decrease in RBM3 at the long term (24h). CSPs are constitutively expressed in multiple organs, such as the retina (Larrayoz et al., 2016), the central nervous system (Liu et al., 2010), or the testes (Xia et al., 2012), and are well conserved among vertebrate species, being especially relevant among hibernating organisms (Sugimoto and Jiang, 2008). Furthermore, the articles providing datasets for the data mining exercise show that CSPs are also abundant in the kidney. Taken together, these data suggest that the involvement of the CSPs in the mechanism of shear stress sensing is a common feature in cell biology that warrants further studies.

Our proposal that CSPs may constitute the link between hypothermia/shear stress and morphological changes in the primary cilia is mainly based on observational data. A formal mechanistic demonstration of this phenomenon must include studies in knockout models for each CSP. In an attempt to provide some mechanistic connection, we have employed a hypothermia mimetic small molecule, zr17-2, which has been shown to increase CIRP expression in R28 cells (Coderch et al., 2017). The application of this molecule in the absence of hypothermia or shear stress has resulted in significant reductions in primary cilia number and length, thus suggesting that CIRP is involved in these phenomena, although we cannot rule out some off-target effects of the small molecule.

In conclusion, we have shown that CSPs are located in the basal body of the primary cilia and cellular centrosome; that hypothermia and shear stress induce a reduction in both the number and the size of primary cilia; and that shear stress induces the expression of CSPs in a complex pattern. All together, these results indicate that cold sensing may constitute a new function of the primary cilium and that the cold-sensing proteins are part of the signal transduction mechanism following shear stress.

Acknowledgements. MDC gratefully acknowledges Gobierno de La Rioja for a predoctoral fellowship. This project was funded by Fundación Rioja Salud (Onco1). IO and SO acknowledge financial support from the “Moore4Medical” project funded by the ECSEL Joint Undertaking under grant agreement H2020-ECSEL-2019-IA-876190.

Conflict of interest. The authors declare that the research was conducted in the absence of any commercial or financial relationships that could be construed as a potential conflict of interest.

References.

Andreu-Cervera A., Catala M. and Schneider-Maunoury S. (2021). Cilia, ciliopathies and hedgehog-related forebrain developmental disorders. Neurobiol. Dis. 150, 105236.

Anvarian Z., Mykytyn K., Mukhopadhyay S., Pedersen L.B. and Christensen S.T. (2019). Cellular signalling by primary cilia in development, organ function and disease. Nat. Rev. Nephrol. 15, 199-219.

Arslanhan M.D., Gulensoy D. and Firat-Karalar E.N. (2020). A Proximity Mapping Journey into the Biology of the Mammalian Centrosome/Cilium Complex. Cells 9, 1390.

Baba T., Nishimura M., Kuwahara Y., Ueda N., Naitoh S., Kume M., Yamamoto Y., Fujita J., Funae Y. and Fukumoto M. (2008). Analysis of gene and protein expression of cytochrome P450 and stress-associated molecules in rat liver after spaceflight. Pathol. Int. 58, 589-595.

Barbosa-Morais N.L., Carmo-Fonseca M. and Aparicio S. (2006). Systematic genome-wide annotation of spliceosomal proteins reveals differential gene family expansion. Genome Res. 16, 66-77.

Chen H.Y., Kelley R.A., Li T. and Swaroop A. (2021). Primary cilia biogenesis and associated retinal ciliopathies. Semin. Cell. Dev. Biol. 110, 70-88.

Coderch C., Diaz de Cerio M., Zapico J.M., Pelaez R., Larrayoz I.M., Ramos A., Martinez A. and de Pascual-Teresa B. (2017). In silico identification and in vivo characterization of small molecule therapeutic hypothermia mimetics. Bioorg. Med. Chem. 25, 6597-6604.

Contartese D.S., Rey-Funes M., Pelaez R., Solino M., Fernandez J.C., Nakamura R., Ciranna N.S., Sarotto A., Dorfman V.B., Lopez-Costa J.J., Zapico J.M., Ramos A., de Pascual-Teresa B., Larrayoz I.M., Loidl C.F. and Martinez A. (2023). A hypothermia mimetic molecule (zr17-2) reduces ganglion cell death and electroretinogram distortion in a rat model of intraorbital optic nerve crush (IONC). Front. Pharmacol. 14, 1112318.

De L.F., Zhang T., Wauquier C., Huez G., Kruys V. and Gueydan C. (2007). The cold-inducible RNA-binding protein migrates from the nucleus to cytoplasmic stress granules by a methylation-dependent mechanism and acts as a translational repressor. Exp. Cell Res. 313, 4130-4144.

Dinsmore C. and Reiter J.F. (2016). Endothelial primary cilia inhibit atherosclerosis. EMBO Rep. 17, 156-166.

Espinha L.C., Hoey D.A., Fernandes P.R., Rodrigues H.C. and Jacobs C.R. (2014). Oscillatory fluid flow influences primary cilia and microtubule mechanics. Cytoskeleton (Hoboken) 71, 435-445.

Garcia G., Raleigh D.R. and Reiter J.F. (2018). How the Ciliary Membrane Is Organized Inside-Out to Communicate Outside-In. Curr. Biol. 28, R421-R434.

Goggolidou P. (2014). Wnt and planar cell polarity signaling in cystic renal disease. Organogenesis 10, 86-95.

Gomez-Ferreria M.A., Rath U., Buster D.W., Chanda S.K., Caldwell J.S., Rines D.R. and Sharp D.J. (2007). Human Cep192 is required for mitotic centrosome and spindle assembly. Curr. Biol. 17, 1960-1966.

Graser S., Stierhof Y.D. and Nigg E.A. (2007). Cep68 and Cep215 (Cdk5rap2) are required for centrosome cohesion. J. Cell Sci. 120, 4321-4331.

Habbig S., Bartram M.P., Muller R.U., Schwarz R., Andriopoulos N., Chen S., Sagmuller J.G., Hoehne M., Burst V., Liebau M.C., Reinhardt H.C., Benzing T. and Schermer B. (2011). NPHP4, a cilia-associated protein, negatively regulates the Hippo pathway. J. Cell Biol. 193, 633-642.

Hagiwara H., Kano A., Aoki T., Ohwada N. and Takata K. (2000). Localization of gamma-tubulin to the basal foot associated with the basal body extending a cilium. Histochem. J. 32, 669-671.

Han S.J., Jung J.K., Im S.S., Lee S.R., Jang B.C., Park K.M. and Kim J.I. (2018). Deficiency of primary cilia in kidney epithelial cells induces epithelial to mesenchymal transition. Biochem. Biophys. Res. Commun. 496, 450-454.

Heydeck W., Fievet L., Davis E.E. and Katsanis N. (2018). The complexity of the cilium: spatiotemporal diversity of an ancient organelle. Curr. Opin. Cell Biol. 55, 139-149.

Hildebrandt F., Benzing T. and Katsanis N. (2011). Ciliopathies. N. Engl. J. Med. 364, 1533-1543.

Iring A., Jin Y.J., Albarran-Juarez J., Siragusa M., Wang S., Dancs P.T., Nakayama A., Tonack S., Chen M., Kunne C., Sokol A.M., Gunther S., Martinez A., Fleming I., Wettschureck N., Graumann J., Weinstein L.S. and Offermanns S. (2019). Shear stress-induced endothelial adrenomedullin signaling regulates vascular tone and blood pressure. J. Clin. Invest. 129, 2775-2791.

Kunnen S.J., Malas T.B., Semeins C.M., Bakker A.D. and Peters D.J.M. (2018). Comprehensive transcriptome analysis of fluid shear stress altered gene expression in renal epithelial cells. J. Cell. Physiol. 233, 3615-3628.

Larrayoz I.M., de Luis A., Rua O., Velilla S., Cabello J. and Martinez A. (2012). Molecular effects of doxycycline treatment on pterygium as revealed by massive transcriptome sequencing. PLoS One 7, e39359.

Larrayoz I.M., Rey-Funes M., Contartese D.S., Rolon F., Sarotto A., Dorfman V.B., Loidl C.F. and Martinez A. (2016). Cold shock proteins are expressed in the retina following exposure to low temperatures. PLoS One 11, e0161458.

Lerit D.A. (2022). Signed, sealed, and delivered: RNA localization and translation at centrosomes. Mol. Biol. Cell 33, pe3

Liu A., Zhang Z., Li A. and Xue J. (2010). Effects of hypothermia and cerebral ischemia on cold-inducible RNA-binding protein mRNA expression in rat brain. Brain Res. 1347, 104-110

Liu H., Kiseleva A.A. and Golemis E.A. (2018). Ciliary signalling in cancer. Nat. Rev. Cancer 18, 511-524.

Liu Y., Hu W., Murakawa Y., Yin J., Wang G., Landthaler M. and Yan J. (2013). Cold-induced RNA-binding proteins regulate circadian gene expression by controlling alternative polyadenylation. Sci. Rep. 3, 2054.

Lleonart M.E. (2010). A new generation of proto-oncogenes: cold-inducible RNA binding proteins. Biochim. Biophys. Acta 1805, 43-52.

Luu V.Z., Chowdhury B., Al-Omran M., Hess D.A. and Verma S. (2018). Role of endothelial primary cilia as fluid mechanosensors on vascular health. Atherosclerosis 275, 196-204.

Maslyk M., Zapico J.M., Swider R.M.-S.S., Ramos A. and de Pascual-Teresa B. (2010). In search of a new prototype in CK2 inhibitors design. Arkivoc 3, 54-71.

Mohammed S.G., Arjona F.J., Verschuren E.H.J., Bakey Z., Alkema W., van H.S., Schmidts M., Bindels R.J.M. and Hoenderop J.G.J. (2018). Primary cilia-regulated transcriptome in the renal collecting duct. FASEB J. 32, 3653-3668.

O'Neill A.C., Uzbas F., Antognolli G., Merino F., Draganova K., Jack A., Zhang S., Pedini G., Schessner J.P., Cramer K., Schepers A., Metzger F., Esgleas M., Smialowski P., Guerrini R., Falk S., Feederle R., Freytag S., Wang Z., Bahlo M., Jungmann R., Bagni C., Borner G.H.H., Robertson S.P., Hauck S.M. and Gotz M. (2022). Spatial centrosome proteome of human neural cells uncovers disease-relevant heterogeneity. Science 376, eabf9088.

Park K.M. (2018). Can tissue cilia lengths and urine cilia proteins be markers of kidney diseases?. Chonnam. Med. J. 54, 83-89.

Pigino G. (2021). Intraflagellar transport. Curr. Biol. 31, R530-R536.

Qiao C., Meng F., Jang I., Jo H., Chen Y.E. and Zhang J. (2016). Deep transcriptomic profiling reveals the similarity between endothelial cells cultured under static and oscillatory shear stress conditions. Physiol. Genomics 48, 660-666.

Rey-Funes M., Contartese D.S., Pelaez R., Garcia-Sanmartin J., Narro-Iniguez J., Solino M., Fernandez J.C., Sarotto A., Ciranna N.S., Lopez-Costa J.J., Dorfman V.B., Larrayoz I.M., Loidl C.F. and Martinez A. (2021). Hypothermic shock applied after perinatal asphyxia prevents retinal damage in rats. Front. Pharmacol. 12, 651599.

Rey-Funes M., Larrayoz I.M., Contartese D.S., Solino M., Sarotto A., Bustelo M., Bruno M., Dorfman V.B., Loidl C.F. and Martinez A. (2017). Hypothermia prevents retinal damage generated by optic nerve trauma in the rat. Sci. Rep. 7, 6966.

Roberts M.S., Sahni J.M., Schrock M.S., Piemonte K.M., Weber-Bonk K.L., Seachrist D.D., Avril S., Anstine L.J., Singh S., Sizemore S.T., Varadan V., Summers M.K. and Keri R.A. (2020). LIN9 and NEK2 are core regulators of mitotic fidelity that can be therapeutically targeted to overcome taxane resistance. Cancer Res. 80, 1693-1706.

Roux E., Bougaran P., Dufourcq P. and Couffinhal T. (2020). Fluid shear stress sensing by the endothelial layer. Front. Physiol. 11, 861.

Sanchez-Duffhues G., de Vinuesa A.G., Lindeman J.H., Mulder-Stapel A., DeRuiter M.C., Van M.C., Goumans M.J., Hierck B.P. and Ten D.P. (2015). SLUG is expressed in endothelial cells lacking primary cilia to promote cellular calcification. Arterioscler. Thromb. Vasc. Biol. 35, 616-627.

Seigel G.M. (2014). Review: R28 retinal precursor cells: the first 20 years. Mol. Vis. 20, 301-306.

Shah P.S., Ohlsson A. and Perlman M. (2007). Hypothermia to treat neonatal hypoxic ischemic encephalopathy: systematic review. Arch. Pediatr. Adolesc. Med. 161, 951-958.

Shida T., Cueva J.G., Xu Z., Goodman M.B. and Nachury M.V. (2010). The major alpha-tubulin K40 acetyltransferase alphaTAT1 promotes rapid ciliogenesis and efficient mechanosensation. Proc. Natl. Acad. Sci. USA 107, 21517-21522.

Smith Q., Macklin B., Chan X.Y., Jones H., Trempel M., Yoder M.C. and Gerecht S. (2018). Differential HDAC6 activity modulates ciliogenesis and subsequent mechanosensing of endothelial cells derived from pluripotent stem cells. Cell Rep. 24, 1930.

Sorokin S. (1962). Centrioles and the formation of rudimentary cilia by fibroblasts and smooth muscle cells. J. Cell Biol. 15, 363-377.

Spasic M. and Jacobs C.R. (2017). Primary cilia: Cell and molecular mechanosensors directing whole tissue function. Semin. Cell. Dev. Biol. 71, 42-52.

Sugimoto K. and Jiang H. (2008). Cold stress and light signals induce the expression of cold-inducible RNA binding protein (cirp) in the brain and eye of the Japanese treefrog (Hyla japonica). Comp. Biochem. Physiol. A. Mol. Integr. Physiol. 151, 628-636.

Uzbekov R.E. and Avidor-Reiss T. (2020). Principal Postulates of Centrosomal Biology. Version 2020. Cells 9, 2156.

Wang W., Jack B.M., Wang H.H., Kavanaugh M.A., Maser R.L. and Tran P.V. (2021a). Intraflagellar transport proteins as regulators of primary cilia length. Front. Cell. Dev. Biol. 9, 661350.

Wang Z.M., Gao X.F., Zhang J.J. and Chen S.L. (2021b). Primary cilia and atherosclerosis. Front. Physiol. 12, 640774.

Wellmann S., Buhrer C., Moderegger E., Zelmer A., Kirschner R., Koehne P., Fujita J. and Seeger K. (2004). Oxygen-regulated expression of the RNA-binding proteins RBM3 and CIRP by a HIF-1-independent mechanism. J. Cell Sci. 117, 1785-1794.

Wellmann S., Truss M., Bruder E., Tornillo L., Zelmer A., Seeger K. and Buhrer C. (2010). The RNA-binding protein RBM3 is required for cell proliferation and protects against serum deprivation-induced cell death. Pediatr. Res. 67, 35-41.

Wheway G., Nazlamova L. and Hancock J.T. (2018). Signaling through the primary cilium. Front. Cell. Dev. Biol. 6, 8.

Wheway G., Nazlamova L., Turner D. and Cross S. (2019). 661W photoreceptor cell line as a cell model for studying retinal ciliopathies. Front. Genet. 10, 308.

Wheway G., Schmidts M., Mans D.A., Szymanska K., Nguyen T.T., et al. (2015). An siRNA-based functional genomics screen for the identification of regulators of ciliogenesis and ciliopathy genes. Nat. Cell Biol. 17, 1074-1087.

Wilsch-Brauninger M. and Huttner W.B. (2021). Primary cilia and centrosomes in neocortex development. Front. Neurosci. 15, 755867.

Wu L., Sun H.L., Gao Y., Hui K.L., Xu M.M., Zhong H. and Duan M.L. (2017). Therapeutic hypothermia enhances cold-Inducible RNA-Binding protein expression and inhibits mitochondrial apoptosis in a rat model of cardiac arrest. Mol. Neurobiol. 54, 2697-2705.

Xia Z., Zheng X., Zheng H., Liu X., Yang Z. and Wang X. (2012). Cold-inducible RNA-binding protein (CIRP) regulates target mRNA stabilization in the mouse testis. FEBS Lett. 586, 3299-3308.

Zein-Sabatto H. and Lerit D.A. (2021). The identification and functional analysis of mRNA localizing to centrosomes. Front. Cell. Dev. Biol. 9, 782802.

Zhang H.T., Xue J.H., Zhang Z.W., Kong H.B., Liu A.J., Li S.C. and Xu D.G. (2015). Cold-inducible RNA-binding protein inhibits neuron apoptosis through the suppression of mitochondrial apoptosis. Brain Res. 1622, 474-483.

Zhu X., Buhrer C. and Wellmann S. (2016). Cold-inducible proteins CIRP and RBM3, a unique couple with activities far beyond the cold. Cell. Mol. Life Sci. 73, 3839-3859.

Tables.

Table 1. Antibodies used for immunofluorescence (IF) staining and Western blotting (WB).

Primary antibodies				
Application	Target protein	Commercial vendor	Reference	RRID
IF, WB	CIRP (rabbit polyclonal)	Proteintech	10209-2-AP	AB_2080263
IF, WB	CIRP (rabbit monoclonal)	Abcam	Ab246510	AB_2923244
IF, WB	RBM3 (rabbit)	Abcam	Ab134946	AB_2892665
IF	Gamma-tubulin (mouse), bound to Alexa 488	Abcam	Ab205475	AB_2889220
IF	Acetylated alpha-tubulin (mouse)	Santa Cruz	Sc-23950	AB_628409
WB	Beta-tubulin (mouse)	Sigma	T4026	AB_477577
Secondary and blocking antibodies				
Application	Specificity	Commercial vendor	Reference	RRID

IF	CF543 (anti mouse IgG)	Biotium	20305	AB_2923245
IF	ALEXA Fluor 647 (anti rabbit IgG)	Invitrogen	A32733	AB_2633282
IF	AffiniPure Fab fragment donkey anti mouse IgG	Jackson Immunoresearch	715-007-003	AB_2307338
WB	HRP-goat anti rabbit IgG	Cell Signaling	7074	AB_2099233
WB	HRP-donkey anti mouse IgG	Jackson Immunoresearch	715-035-151	AB_2340771

Table 2. Primers used for quantitative real-time PCR. All sequences were taken from the rat genome.

Gene of interest	Sense primer	Antisense primer	Annealing temperature
CIRP	AGACTACTATGCCAGCCGGA	AGCTGTCTCTGTAGGACCCA	60 °C
RBM3	TGGAGAGTCCCTGGATGGG	TGGTTCCCCTGGCAGACTT	60 °C
GAPDH	ATGGTGAAGGTCGGTGTGAAC	TCTCAGCCTTGACTGTGCC	60 °C

Figure legends.

Figure 1. Representative confocal microscopy images showing colocalization of CIRP with γ-tubulin in the centrosomes and basal bodies of the primary cilia. (**a**) R28 cells were immunostained for CIRP in red, γ-tubulin in green, and acetylated tubulin in purple. The nucleus was stained with Hoechst in blue. The last panel is a merged image of all the previous ones. CIRP labels the cell nucleus but also the basal body (arrows). Scale bar = 5 µm. (**b**) Panoramic view of several R28 cells displaying primary cilia, stained as above. Scale bar = 2.5 µm.

Figure 2. Representative confocal microscopy images showing colocalization of CIRP (**a**) and RBM3 (**b**) with γ-tubulin in the centrosomes and basal bodies of the primary cilia during different stages of the mitosis (prophase, metaphase, anaphase). The staining pattern is the same as in Fig.1. CIRP and RBM3 (red) label the cell nuclei but also the centrosomes and basal bodies (arrows). Scale bars = 10 µm.

Figure 3. Effects of hypothermia on primary cilia. Representative confocal microscopy images of R28 cells exposed to normothermia (37°C) or hypothermia (32°C) for 96h. The staining procedure for CIRP (**a**) and RBM3 (**b**) was the same as in Fig. 1. Scale bars = 5 µm. The percentage of cells containing a primary cilium and the length of these structures was calculated (**c**). Bars represent mean ± standard deviation of all measurements. *: p<0.05; ****: p<0.0001.

Figure 4. Effects of hypothermia and zr17-2 on CIRP expression and on primary cilia morphology. CIRP expression significantly increases in R28 cells exposed to hypothermia (32°C) (**a**). The presence of zr17-2 in the culture medium produces a reduction in the number of primary cilia (**b**) and in their length (**c**). Bars represent mean ± standard deviation of all measurements. *: p<0.05; **: p<0.01; ****: p<0.0001.

Figure 5. Effects of laminar flow on primary cilia. Representative confocal microscopy images of R28 cells exposed to static or laminar flow (62 µl/min) conditions for 8 h and stained for CIRP (**a**) or RBM3 (**b**). The staining procedure was the same as in Fig. 1. Scale bars = 7.5 µm (**a**) or 5 µm (**b**). The percentage of cells containing a primary cilium was calculated (**c**). Bars represent mean ± standard deviation of all measurements. *: p<0.05; **: p<0.01;***: p<0.001.

Figure 6. Gene expression quantification (qRT-PCR) for CIRP (**a**) and RBM3 (**b**) in R28 cells subjected to different flow conditions and times. Bars represent mean ± standard deviation of all measurements. *: p<0.05; **: p<0.01;****: p<0.0001.

Figure 7. Effects of oscillatory flow on primary cilia. Representative confocal microscopy images of R28 cells exposed to static or oscillatory flow conditions for 2 h and stained for CIRP (**a**) or RBM3 (**b**). The staining procedure was the same as in Fig. 1. Scale bars = 5 µm. The percentage of cells containing a primary cilium and the length of these structures was calculated (**c**). Bars represent mean ± standard deviation of all measurements. *: p<0.05; ****: p<0.0001.

Figure 8. Gene (**a**,**b**) and protein (**c**,**d**) expression quantification for CIRP (**a**,**c**) and RBM3 (**b**,**d**) in R28 cells subjected to oscillatory flow conditions at different times. A representative Western blot for CIRP and tubulin is shown for the first time point. Bars represent mean ± standard deviation of all measurements. *: p<0.05; **: p<0.01; ***:p<0.001;****: p<0.0001.

Figure 9. Results of the analysis of previous RNA Seq experiments on shear stress models in renal cell lines. These studies were previously published and are identified by their first authors (Mohammed et al. 2018; Kunnen et al. 2018; Qiao et al. 2016). They were performed with different flow conditions (0.6, 1.9, and 5.0 dynes/cm^2 respectively) and times of exposure (3, 6, and 24 h). The first two studies correspond to laminar flow whereas the third one used oscillatory flow. Bars represent mean ± standard deviation of all measurements. *: p<0.05.

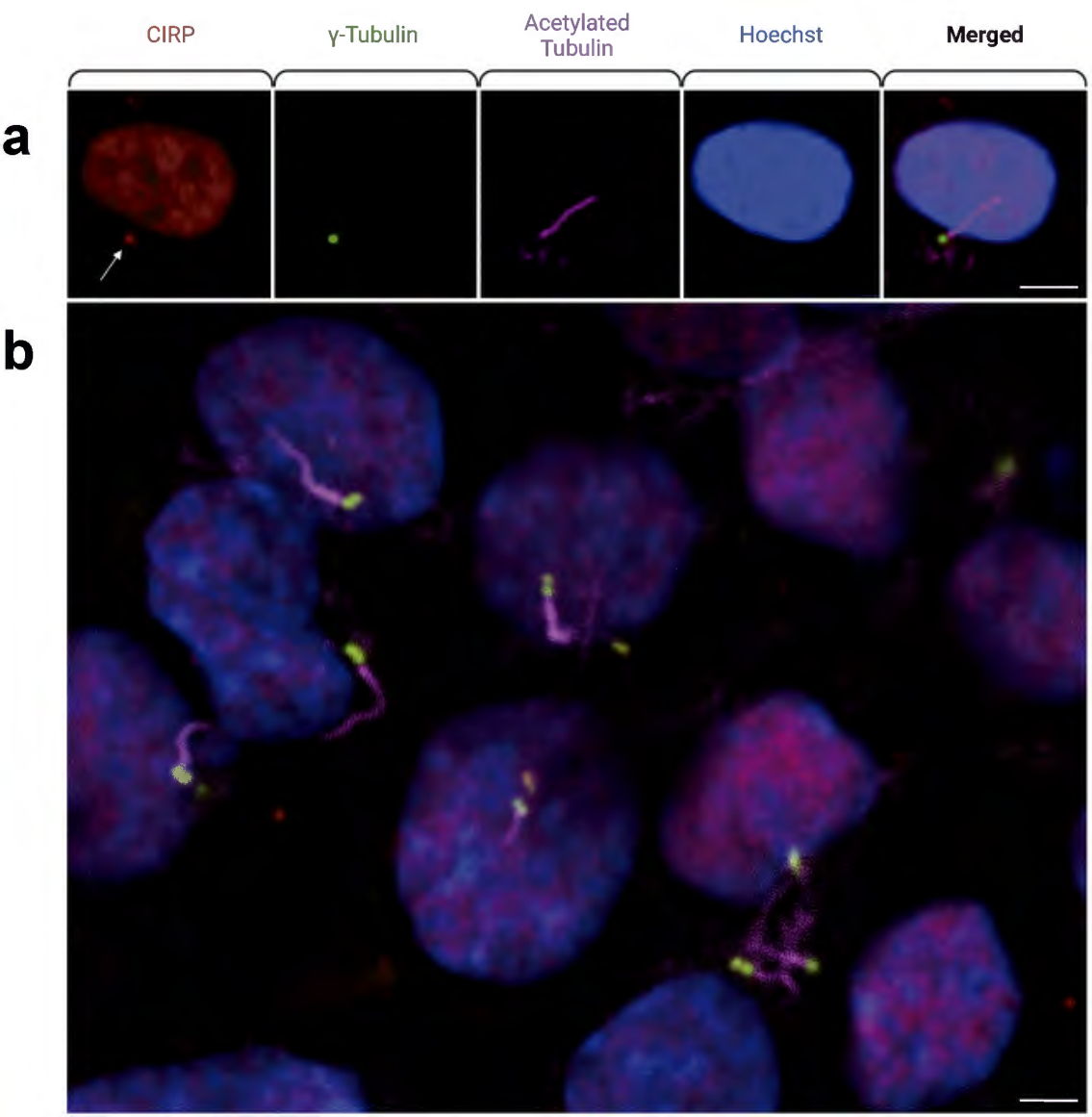
CIRP
γ-Tubulin
Acetylated Tubulin
Hoechst
Merged
a
b

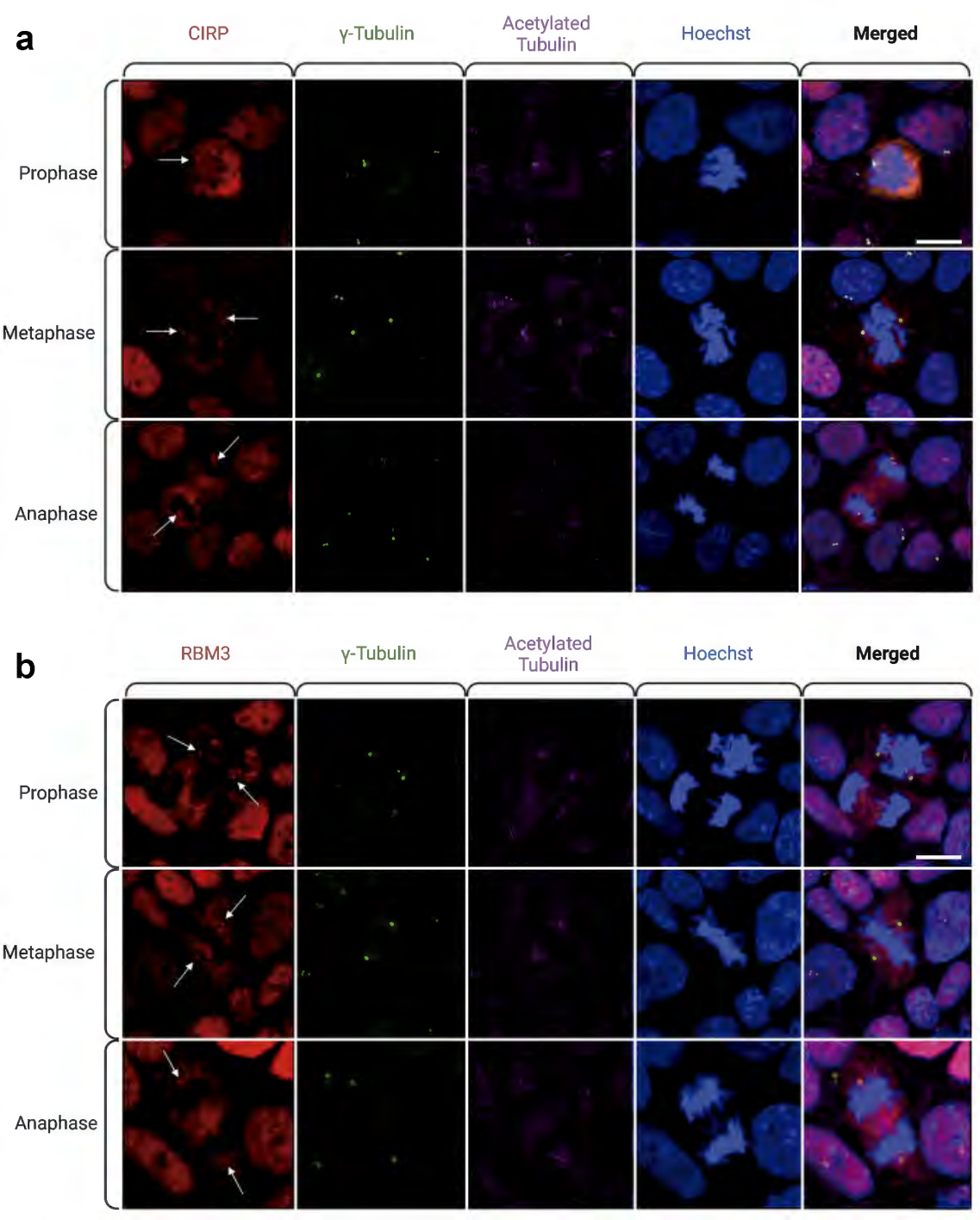
a
CIRP
γ-Tubulin
Acetylated Tubulin
Hoechst
Merged
Prophase
Metaphase
Anaphase
b
RBM3
γ-Tubulin
Acetylated Tubulin
Hoechst
Merged
Prophase
Metaphase
Anaphase

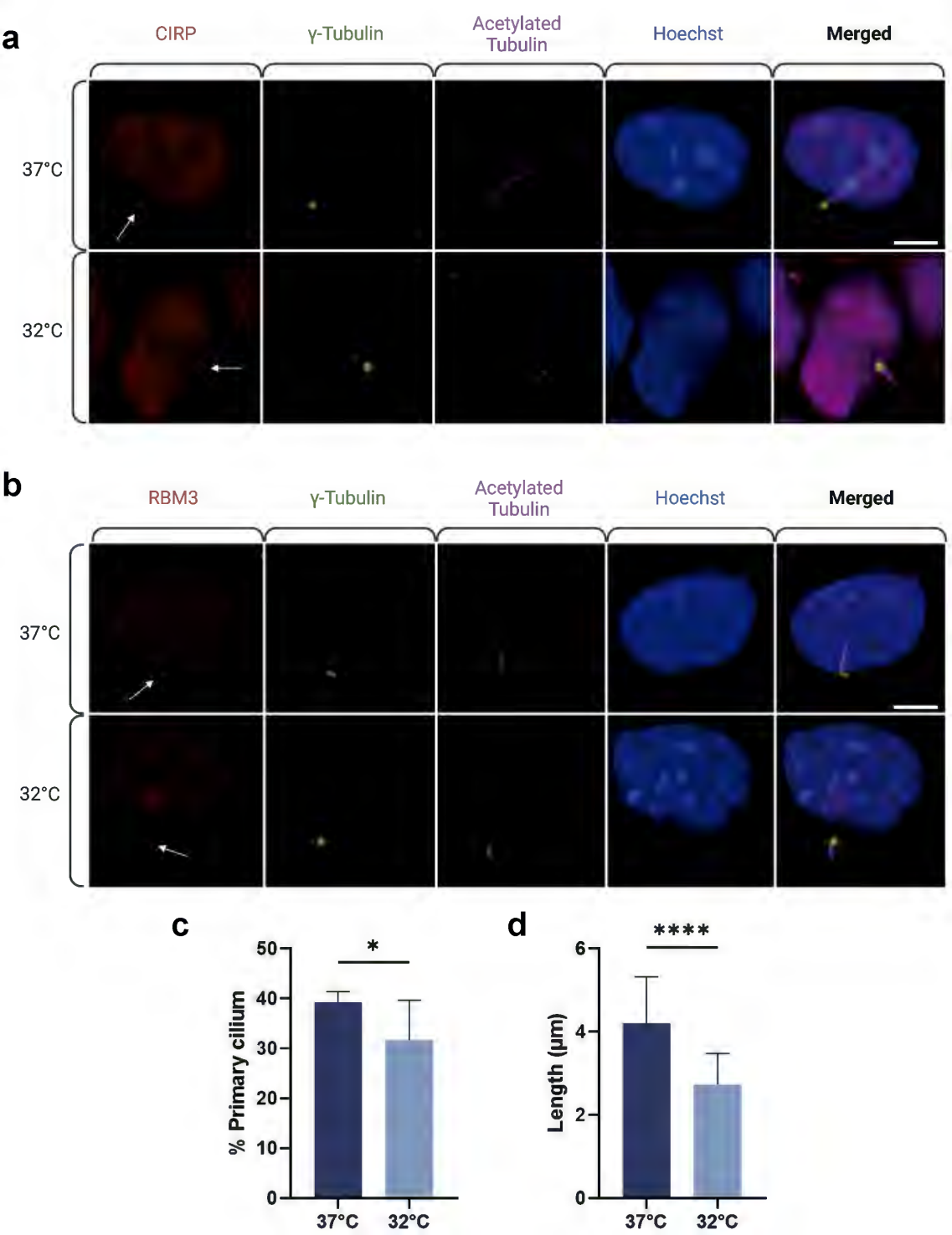
a
CIRP
γ-Tubulin
Acetylated Tubulin
Hoechst
Merged
37°C
32°C
b
RBM3
γ-Tubulin
Acetylated Tubulin
Hoechst
Merged
37°C
32°C
c
*
% Primary cilium
50
40
30
20
10
0
37°C
32°C
d
****
Length (μm)
6
4
2
0
37°C
32°C

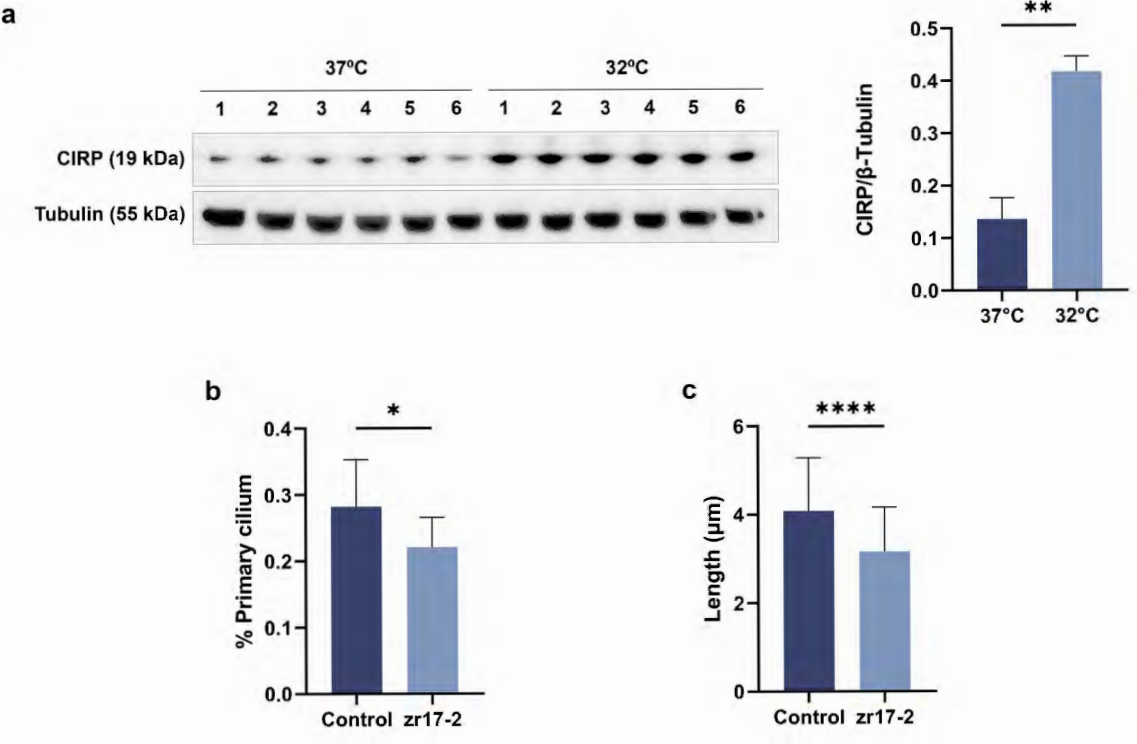
a
37ºC
32ºC
1 2 3 4 5 6 1 2 3 4 5 6
CIRP (19 kDa)
Tubulin (55 kDa)
**
CIRP/β-Tubulin
0.5
0.4
0.3
0.2
0.1
0.0
37°C
32°C
b
*
% Primary cilium
0.4
0.3
0.2
0.1
0.0
Control
zr17-2
c
****
Length (μm)
6
4
2
0
Control
zr17-2

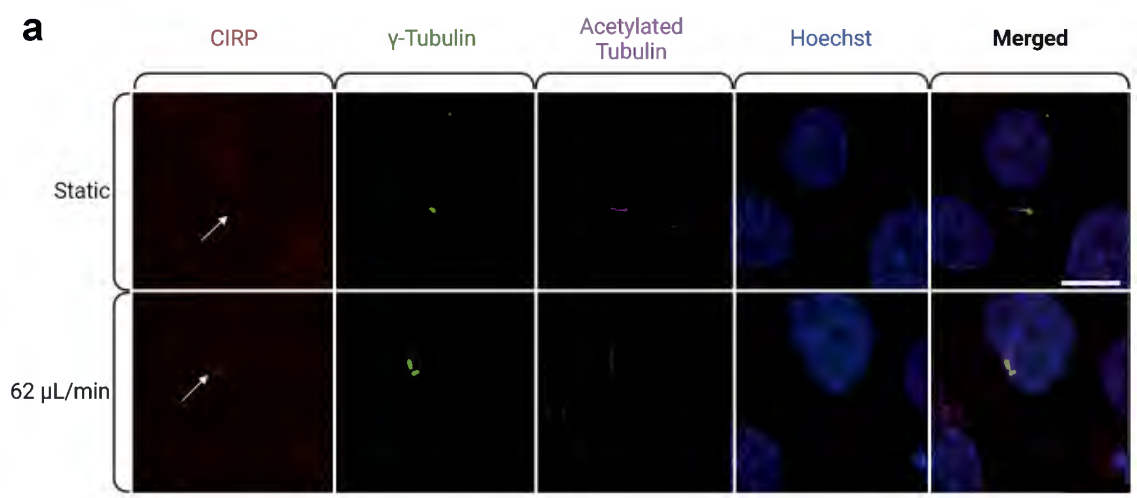
a
CIRP
γ-Tubulin
Acetylated Tubulin
Hoechst
Merged
Static
62 µL/min

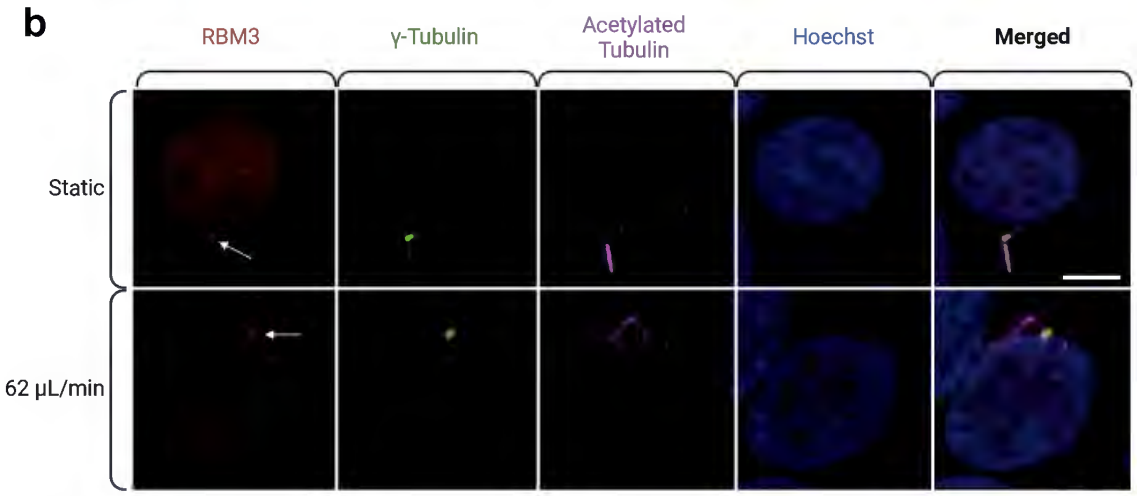
b
RBM3
γ-Tubulin
Acetylated Tubulin
Hoechst
Merged
Static
62 µL/min

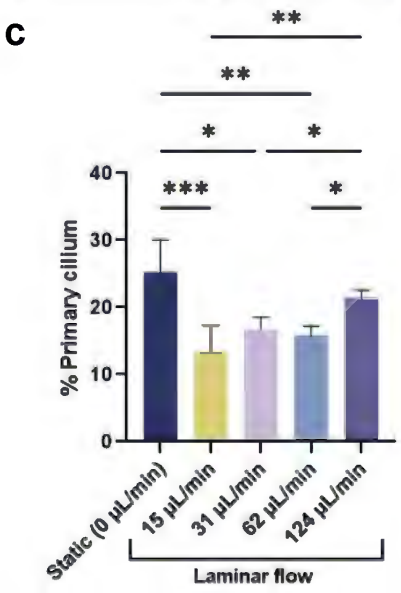
c
**
**
*
*
***
*
40
30
20
10
0
% Primary cilium
Static (0 µL/min)
15 µL/min
31 µL/min
62 µL/min
124 µL/min
Laminar flow

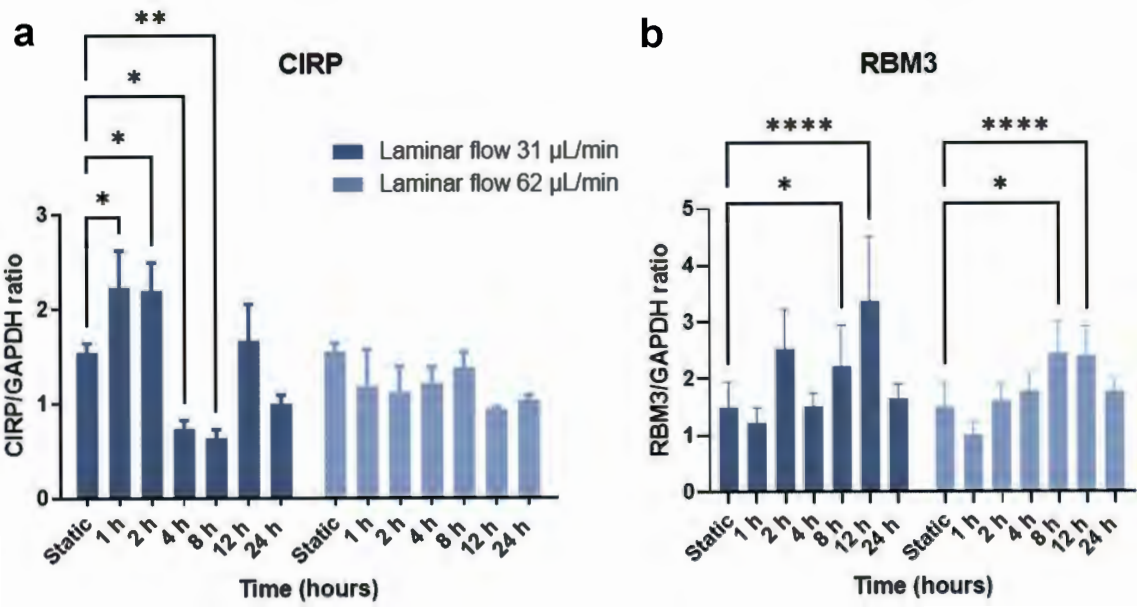
a
CIRP
Laminar flow 31 µL/min
Laminar flow 62 µL/min
CIRP/GAPDH ratio
Static
1 h
2 h
4 h
8 h
12 h
24 h
Time (hours)
b
RBM3
RBM3/GAPDH ratio
Time (hours)

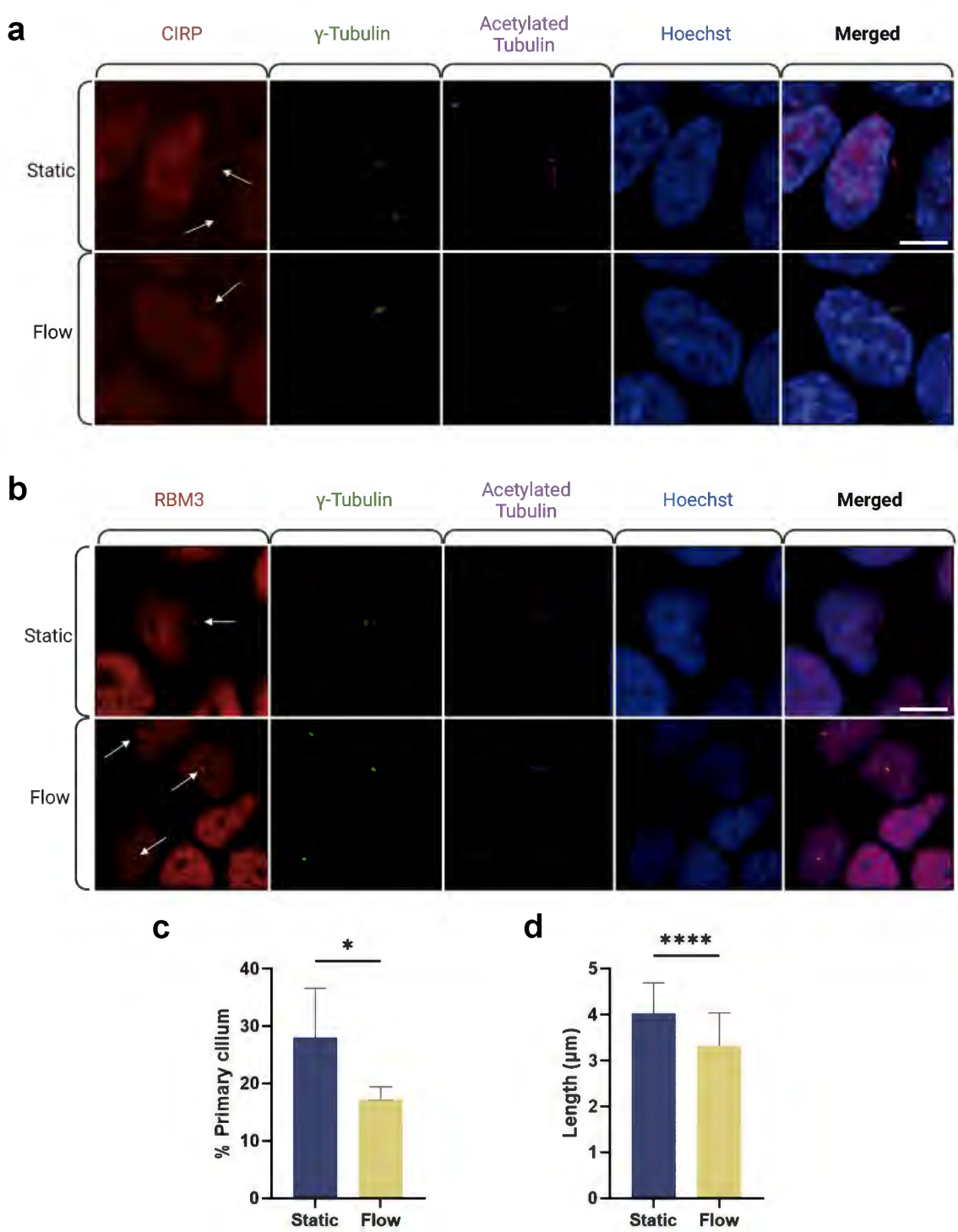
a
CIRP
γ-Tubulin
Acetylated Tubulin
Hoechst
Merged
Static
Flow
b
RBM3
γ-Tubulin
Acetylated Tubulin
Hoechst
Merged
Static
Flow
c
*
% Primary cillum
40
30
20
10
0
Static
Flow
d
****
Length (µm)
5
4
3
2
1
0
Static
Flow

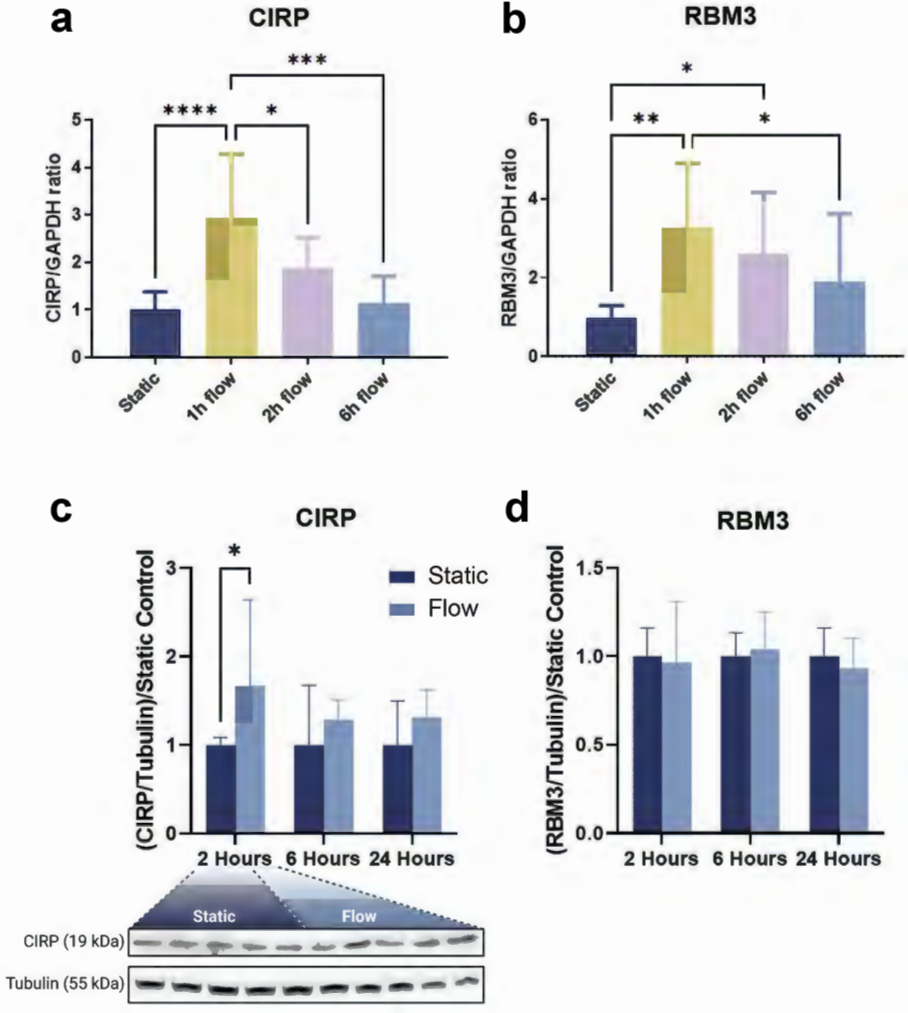
a
CIRP
CIRP/GAPDH ratio
****
*
***
Static
1h flow
2h flow
6h flow
b
RBM3
RBM3/GAPDH ratio
**
*
*
c
CIRP
(CIRP/Tubulin)/Static Control
Static
Flow
2 Hours
6 Hours
24 Hours
CIRP (19 kDa)
Tubulin (55 kDa)
d
RBM3
(RBM3/Tubulin)/Static Control

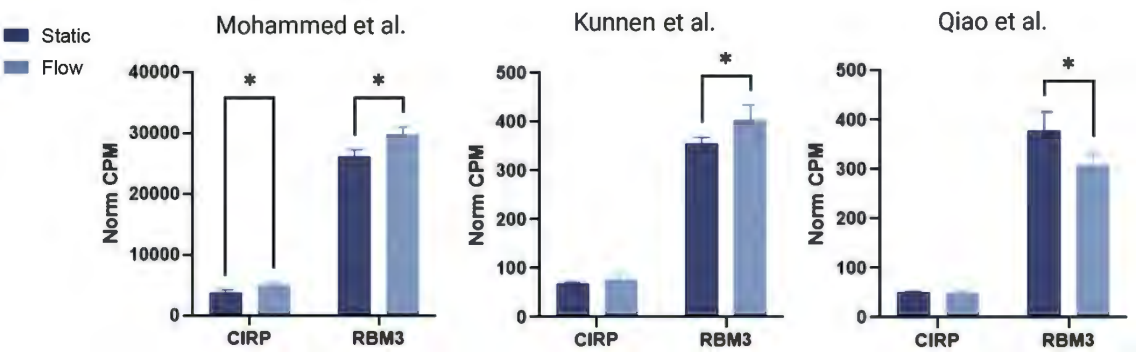
Static
Flow
Mohammed et al.
Kunnen et al.
Qiao et al.
Norm CPM
40000
30000
20000
10000
0
500
400
300
200
100
*
CIRP
RBM3